
Accelerating Stochastic Simulation with Interactive Neural Processes

Dongxia Wu

University of California San Diego
La Jolla, CA
dowu@ucsd.edu

Matteo Chinazzi

Northeastern University
Boston, MA
m.chinazzi@northeastern.edu

Alessandro Vespignani

Northeastern University
Boston, MA
a.vespignani@northeastern.edu

Yi-An Ma

University of California San Diego
La Jolla, CA
yianma@ucsd.edu

Rose Yu

University of California San Diego
La Jolla, CA
roseyu@ucsd.edu

Abstract

Stochastic simulations such as large-scale, spatiotemporal, age-structured epidemic models are computationally expensive at fine-grained resolution. We propose Interactive Neural Process (INP), an interactive framework to continuously learn a deep learning surrogate model and accelerate simulation. Our framework is based on the novel integration of Bayesian active learning, stochastic simulation and deep sequence modeling. In particular, we develop a novel spatiotemporal neural process model to mimic the underlying process dynamics. Our model automatically infers the latent process which describes the intrinsic uncertainty of the simulator. This also gives rise to a new acquisition function that can quantify the uncertainty of deep learning predictions. We design Bayesian active learning algorithms to iteratively query the simulator, gather more data, and continuously improve the model. We perform theoretical analysis and demonstrate that our approach reduces sample complexity compared with random sampling in high dimension. Empirically, we demonstrate our framework can faithfully imitate the behavior of a complex infectious disease simulator with a small number of examples, enabling rapid simulation and scenario exploration.

1 Introduction

Computational modeling is now more than ever at the forefront of infectious disease research due to the COVID-19 pandemic. Large-scale stochastic simulations play a critical role in understanding and forecasting infectious disease dynamics, creating what-if scenarios, and informing public health policy making. More broadly, stochastic simulation [35, 2] produces forecasts about complex interactions among people, environment, space, and time given a set of parameters. They provide the numerical tools to simulate probabilistic models and stochastic processes in finance [22], chemistry [13] and many scientific disciplines.

Unfortunately, stochastic simulations at fine-grained spatial and temporal resolution are extremely computationally expensive. For example, epidemic models whose aim is to simulate realistic

diffusion dynamics via in-silico experiments require the exploration of a large parameter space (e.g. characteristics of a virus or policy changes). Therefore, hundreds of thousands of simulations are required to explore and calibrate the epidemic model with observed epidemic surveillance data. This process significantly hinders the adaptive capability of existing stochastic simulators, especially in “war time” emergencies, due to the lead time needed to execute new simulations and produce actionable insights that could help guide decision makers.

Learning data-driven surrogate models to speed up complex simulation has been explored in climate modeling and fluid dynamics [36, 41, 16, 34] for deterministic partial differential equations (PDEs). But stochastic simulation has not been considered extensively in the machine learning literature. Furthermore, these surrogate models only approximate the dynamics of the PDEs to predict the future, but lack the controlled generation capability offered by the simulators. More importantly, the majority of the surrogate models are trained *passively* using a given set of simulation data. There is no interaction between the surrogate model and the simulator. This requires a large number of simulations to cover different parameter regimes of the simulator and ensure generalization.

We propose a Bayesian active learning framework to speed up the stochastic simulation of infectious diseases. Given parameters such as disease reproduction rate, mobility dynamics, as well as initial state, current mechanistic simulators generate future outbreak states with time-consuming numerical integration. Our framework accelerates the simulation by learning a surrogate model and bypassing numerical integration. Specifically, we develop a novel deep generative model based on neural processes (NP) [12] to mimic the behavior of the mechanistic simulator. To better represent the epidemic dynamics, we extend NP to spatiotemporal setting: it introduces a time-evolving latent process for temporal dynamics and integrates graph convolution for spatial modeling.

To adapt to the rapidly changing dynamics, we propose a novel active learning algorithm to interact with the simulator and update our model in “real-time”. Based on neural process, we derive a new acquisition function, MaxZdiff, to quantify the prediction uncertainty on the latent process and select the parameters. We then query the simulator with the selected parameters to generate new simulation data and continuously improve our model. Compared with Gaussian processes, a common tool for active learning, INP is more expressive, more accurate, and scales easily to high-dimensional sequence data. We provide theoretical guarantees for the sample efficiency of this procedure over random sampling. We also demonstrate the efficacy of our method on large-scale spatiotemporal epidemic models. In summary, our contributions include:

- An interactive framework with Bayesian active learning for accelerating stochastic simulation with few examples
- Novel deep generative model as a more flexible and scalable alternative to Gaussian processes for uncertainty quantification.
- Extension of neural process to spatiotemporal settings as a deep surrogate model for large-scale, stochastic, spatiotemporal epidemic models
- New acquisition function based on the inferred latent process with theoretical guarantees

2 Methodology

Consider a stochastic process $\{X(t) : t \in [0, T]\}$, governed by an unknown dynamics with time-varying parameters $\theta(t) \in \mathbb{R}^K$ and the initial state $x_0 \in \mathbb{R}^D$. We obtain realizations from the stochastic process as sequences (x_1, x_2, \dots, x_t) . In epidemic modeling, $\theta(t)$ can represent the effective reproduction rate of the virus at a given point in time, the contact rates between individuals belonging to different age groups, the people’s degree of short- or long-range mobility, or the effects of time varying policy interventions (e.g. non-pharmaceutical interventions). The state x_t includes both the daily prevalence and daily incidence for each compartment of the epidemic model (e.g. number of people that are infectious at time t and number of new infected individuals at time t).

Let $\theta := [x_0, \theta_1, \dots, \theta_t]$ represents the initial condition and the parameters of the stochastic process. Stochastic simulation uses a mechanistic model $F(\theta; \xi)$ to simulate the evolution of $\{X(t)\}$ where the random variable ξ represents the stochasticity in the simulator. However, realistic large-scale stochastic simulations are computationally intensive. In the following section, we describe a pipeline called Interactive Neural Process (INP) to continuously query and interact with the stochastic simulator, in order to learn a surrogate model for rapid simulation.

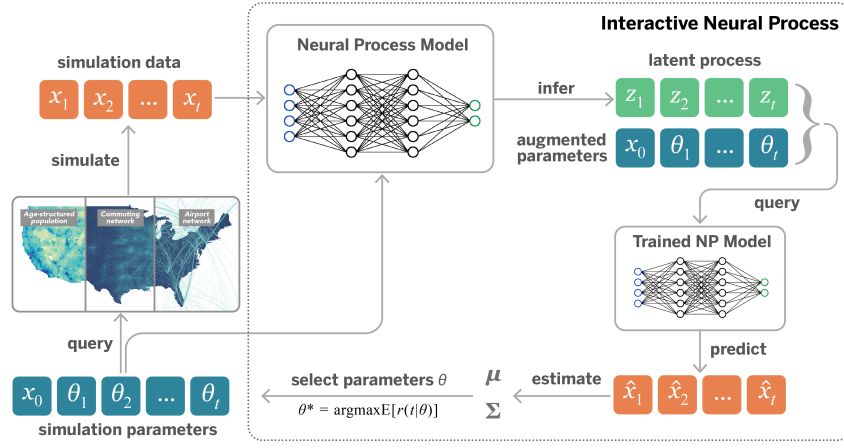


Figure 1: Illustration of the interactive neural process (INP). Given simulation parameters and data, INP trains a Neural Process model to infer the latent process. The inferred latent process allows prediction and uncertainty quantification. The uncertainty is used to select the next set of parameters to query the simulator and simulate more data.

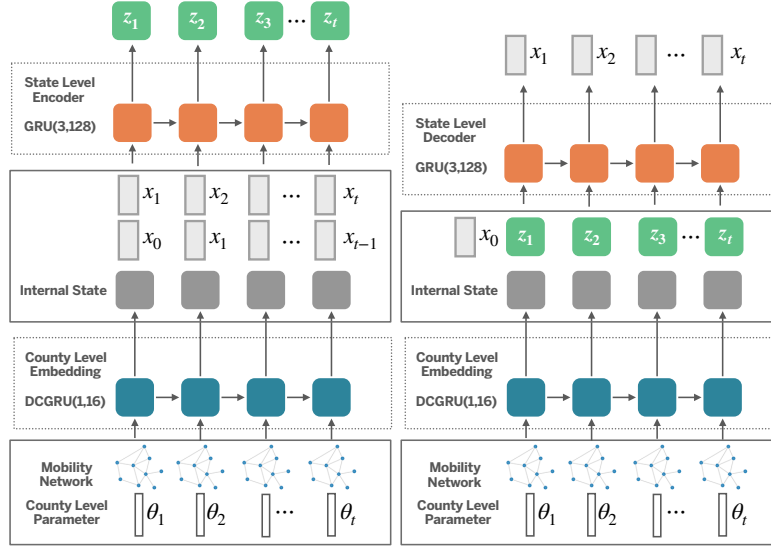


Figure 2: Visualization of the spatiotemporal NP model architecture. For both the encoder and the decoder, we use a diffusion convolutional GRU (DCGRU) [24] to capture spatiotemporal dependency.

2.1 Interactive Neural Process

We describe a hybrid interactive learning framework to speed up stochastic simulation. At a high-level, we train a deep learning surrogate model for the stochastic simulator. Our model directly predicts the future states and bypasses the expensive sampling steps in the simulator. As show in Figure 1, given initial state x_0 and the parameters $(\theta_1, \theta_2, \dots, \theta_t)$, we query the simulator, i.e., the mechanistic epidemic model to obtain a set of simulation data $\{(x_1, x_2, \dots, x_t)\}$. We aim to design a deep generative model that can approximate the distribution of the simulation data. In a way, the deep network becomes a surrogate model that can mimic the internal mechanism of the simulator.

We extend neural process [12] (NP) model to capture the spatiotemporal dynamics in infectious disease. Using the NP model, we can infer the latent process (z_1, z_2, \dots, z_t) which automatically estimate the uncertainty of the surrogate model. During inference, given augmented parameters θ corresponding to different scenarios, we can combine the inferred latent process with the augmented parameters and generate predictions $(\hat{x}_1, \hat{x}_2, \dots, \hat{x}_t)$

To adapt to the rapid changing dynamics, we instantiate Bayesian active learning to iteratively query the simulator for specific parameters and acquire more simulation data. Specifically, we compute the predictive mean μ and covariance Σ based on $(\hat{x}_1, \hat{x}_2, \dots, \hat{x}_t)$ from the current NP model. Then we design a new acquisition function to select the parameters θ where the NP model is uncertainty. We use the selected parameters θ to query the simulator, and in turn generate new simulation to further improve the learning model. Next, we describe each of the components in detail.

2.2 Spatiotemporal Neural Process

Neural process [12] (NP) is a type of generative model that defines distributions over functions. It approximates a stochastic process by combining Gaussian process with deep learning. Given realizations from the stochastic process $X(t; \theta)$ as a function $x(\theta)$, we draw samples from this function and obtain $(\theta, x_{1:t})$. Neural process introduces latent variables z to capture the stochasticity and learns the conditional distribution $p(x_{1:t}|\theta)$ by optimizing the ELBO loss:

$$\log p(x_{1:t}|\theta) \geq \mathbb{E}_{q(z|\theta, x_{1:t})} [\log p(x_{1:t}|z, \theta)] - \text{KL}(q(z|\theta, x_{1:t})||p(z)) \quad (1)$$

Here $p(z)$ is the prior distribution for the latent variable. The prior distribution $p(z)$ is conditioned on a set of training data as context points $\theta^c, x_{1:t}^c$ as $p(z|\theta^c, x_{1:t}^c)$.

However, a vanilla NP model uses a global latent variable z which can be limiting for non-stationary, spatiotemporal dynamics in the epidemics. We propose spatiotemporal neural process (STNP). STNP introduces a time-evolving latent process $Z(t) = (z_1, z_2, \dots, z_t)$ to represent the unknown dynamics. The latent process is higher dimensional than the observed state $X(t)$. It provides a expressive description of the internal mechanism of the stochastic simulator. For spatial dependency, for instance, the travel graph between locations, we use an adjacency matrix $A \in \mathbb{R}^{D \times D}$ where A_{ij} represents the spatial proximity between two locations.

Spatiotemporal neural process models the conditional distribution $p(x_{1:t}|\theta, A)$ given the parameter θ and the spatial information A . We can derive a similar ELBO objective for this distribution.

$$\log p(x_{1:t}|\theta, A) \geq \mathbb{E}_{q(z_{1:t}|\theta, x)} [\log p(x_{1:t}|z_{1:t}, \theta, A)] - \text{KL}(q(z_{1:t}|\theta, x_{1:t}, A)||p(z_{1:t})) \quad (2)$$

where $z_{1:t}$ is the latent process and A is a graph. We can condition the prior distribution on a set of training sequences $p(z_{1:t}|\theta^c, x_{1:t}^c)$ as context.

Model Architecture To implement STNP, we need to approximate the distributions $q(z_{1:t}|\theta, x_{1:t}, A)$ and $p(x_{1:t}|z_{1:t}, \theta, A)$. We use an encoder-decoder architecture. The encoder parametrizes the mean and standard deviation of $q(z_{1:t}|\theta, x_{1:t}, A)$ and we use re-parametrization [20] to sample $z_{1:t}$ from it. The decoder generates $x_{1:t}$ in an auto-regressive fashion.

We instantiate a STNP to mimic an epidemic model which has θ at both county and state level and x_t at the state level. Figure 2 shows the model architecture. We use county-level parameter θ together with a county-to-county mobility graph A as input. To capture the spatiotemporal dependency, we use the Diffusion Convolutional Gated Recurrent Unit (DCGRU) layer [23] which uses graph convolution to embed the graph in a GRU. We use a linear layer to map the county-level output to hidden features h_t at the state level. For both the state-level encoder and decoder, we use multi-layer GRUs. We encode $x_{0:t-1}, x_{1:t}$, and the corresponding hidden features to generate mean and standard deviation for sampling. We use (x_t, z_t, h_t) as input to decode x_{t+1} .

2.3 Bayesian Active Learning

We start with some simulation data $\mathcal{S}_1 = \{\theta^{(1)}, x_{1:t}^{(1)}\}$ to train our NP model. However, as the simulation is expensive, we cannot afford to simulate all possible scenarios beforehand and only passively training the NP model. Instead, we use Bayesian active learning to actively query the data from the stochastic simulator and adapt the model in “real time”.

Algorithm 1 details a Thompson sampling type procedure for Bayesian active learning. Our neural process model automatically infer the variational posterior over the latent process $q(z_{1:t}|x_{1:t}, \theta)$ and approximates the predictive distribution $p(x_{1:t}|z_{1:t}, \theta)$. Since ours is an interactive process, we use the superscript (i) to denote the i -th interaction with the simulator during active learning.

Step 5 in the algorithm is the selection of parameters where the current surrogate model is uncertainty. These parameters would determine where to query the simulator and obtain more training data. We use a generic reward function $r(t|\theta)$ to represent the optimization objective which is time-evolving and depends on the parameters θ . There are multiple options for defining the reward (acquisition function). For example, the reward function $r(t|\theta)$ can either be the log-likelihood of the data, i.e. $r(t|\theta) = \log p(x_{1:t}|\theta)$ or the predictive variance, or the computational cost.

Algorithm 1: Interactive Neural Process

Input: Initial simulation data \mathcal{S}_1

```
1 Train the model  $\text{NP}^{(1)}(\mathcal{S}_1)$  ;  
2 for  $i = 1, 2, \dots$  do  
3   Infer  $(z_1, z_2, \dots, z_t) \sim q^{(i)}(z_{1:t}|x_{1:t}, \theta)$  ;  
4   Predict  $(\hat{x}_1, \hat{x}_2, \dots, \hat{x}_t) \sim p^{(i)}(x_{1:t}|z_{1:t}, \theta)$  ;  
5   Optimize  $\theta^{(i+1)} \leftarrow \arg \max_{\theta} \mathbb{E}_{p(x_{1:t}|z_{1:t}, \theta)} [r(t|\theta)]$  ;  
6    $x_{1:t}^{(i+1)} \leftarrow \text{Query the simulator } F(\theta^{(i+1)}; \xi)$  ;  
7    $\mathcal{S}_{i+1} \leftarrow \mathcal{S}_i \cup \{\theta^{(i+1)}, x_{1:t}^{(i+1)}\}$  ;  
8   Update the model  $\text{NP}^{(i+1)}(\mathcal{S}_{i+1})$  ;  
9 end
```

2.4 Reward/Acquisition functions

There are different strategies to select the next set of parameters to query the stochastic simulator. For regression tasks, standard acquisition functions for active learning include Maximum Mean Standard Deviation (Mean STD), Maximum Entropy, Bayesian Active Learning by Disagreement (BALD), and random sampling. BALD reduces to mean STD for regression. In general, Maximum Entropy is intractable with continuous output. We assume the predictions follow a multivariate Gaussian distribution and compute the maximum entropy approximately. We found empirically that Mean STD often becomes over-conservative and tends to explore less. We thus introduce a new acquisition function based on our unique NP design called Maximum Z Difference (MaxZdiff).

Mean STD. Given the augmented parameter θ and the inferred latent process $z_{1:t}$, we can use our trained neural process model to generate sequence of predictions. For each θ , we can estimate the predictive distribution over $\hat{x}_{1:t}$ by sampling multiple $z_{1:t}$ and generating sequence of predictions $\hat{x}_{1:t}$. For a length T sequence with dimension D , we compute the per time step per feature dimension standard deviation $\sigma_{t,d}$ of these predictions. Mean STD computes $\bar{\sigma} = \frac{1}{TD} \sum_{t=1}^T \sum_{d=1}^D \sigma_{t,d}$ for each parameter. We select the parameter θ with the maximum $\bar{\sigma}$.

Maximum Entropy. We follow the same procedure as Mean STD to generate sequence of predictions. then we compute the covariance $\Sigma \in \mathbb{R}^{TD \times TD}$ using the predictions during inference. We assume the predictions follows multivariate normal distribution to compute the differential entropy for each parameter $h = \frac{1}{2} \ln |\Sigma| + \frac{TD}{2} (1 + \ln 2\pi)$. We select the parameter θ with the maximum entropy.

Maximum Z Difference. Given the learned variational posterior $q^{\text{old}}(z_{1:t}|x_{1:t}, \theta)$ from the previous iteration, we can evaluate it on all the parameters θ remained in the search space. Specifically, for each θ , we generate sequence of predictions $\hat{x}_{1:t}$. Then we use $\hat{x}_{1:t}$ and θ as input to the encoder to re-evaluate the posterior $q(z_{1:t}|\hat{x}_{1:t}, \theta)$. Maximum z difference computes the distributional difference with respect to the latent process $z_{1:t}$ as $d_z = D(q^{\text{old}}(z_{1:t}|x_{1:t}, \theta) \| q(z_{1:t}|\hat{x}_{1:t}, \theta))$ where $D(\cdot \| \cdot)$ denotes the divergence measure. We can use either the KL divergence or the sum of L2 distance mean and standard deviations to quantify the difference. We select the parameter θ with highest score in d_z .

2.5 Theoretical Analysis

We shed light onto the intuition behind choosing adaptive sample selection over random sampling via analyzing a simplifying situation. Assume that at a certain stage we have learned a feature map Ψ which maps the input θ of the neural network to the last layer. Then the output X can be modeled as $X = \langle \Psi(\theta), z^* \rangle + \epsilon$, where z^* is the true hidden variable, ϵ is the random noise.

Our goal is to generate an estimate \hat{z} , and use it to make predictions $\langle \Psi(\theta), \hat{z} \rangle$. A good estimate shall achieve small error in terms of $\|\hat{z}_t - z^*\|_2$ with high probability. In the following theorem, we prove that greedily maximizing the variance of the prediction to choose θ will lead to an error of order $\mathcal{O}(d)$ less than that of random exploration in the space of θ , which is significant in high dimension.

Theorem 1. For random feature map $\Psi(\cdot)$, greedily maximizing the variance of the posterior predictive distribution $\mathbb{E} \left[(\langle \Psi(\theta), \hat{z} \rangle - \mathbb{E} \langle \Psi(\theta), \hat{z} \rangle)^2 \right]$ in search of θ will lead to an error $\|\hat{z}_t - z^*\|_2$ of order $\mathcal{O}(\sigma d / \sqrt{t})$ with high probability.

On the other hand, random sampling of θ will lead to an error of order $\mathcal{O}(\sigma d^2 / \sqrt{t})$ with high probability.

See proofs in the Appendix.

3 Related Work

Bayesian Active Learning. Bayesian Active Learning by Disagreement (BALD) uses predictive entropy to quantify the information gain. Classic work in [17] use Gaussian Process (GP) to compute the predictive distribution. [43] propose an active learning algorithm for time series modeling with GP. For deep learning, the seminal work of [39] use neural networks as an alternative to GPs to model distributions over functions. Deep Bayesian active learning has been studied for image classification [10], entity recognition [37] and sequence labeling [38], but not for stochastic simulation. For PDEs, [32] presents an active learning algorithm to learn a deep neural net surrogate for PDEs based on the predictive uncertainty from the deep ensemble [21]. Our neural process model, however, is generative, and can efficiently infer the latent process from spatiotemporal sequences.

Neural Processes. Neural processes [12] attempts to imbue deep neural networks with the ability of Gaussian processes to capture uncertainty. NP defines distributions over functions using a global latent variable. Attentive NP [19] further introduce Attention to NP in order to alleviate the overfitting. [26] use local latent variables instead and explicitly model their dependencies with a graph. All existing neural processes are learning *passively* from a given dataset, whereas ours consider the *active* setting to interactively learn a NP model.

Stochastic Simulation and Epidemic Modeling Complex simulations are fundamental to many scientific fields [35], especially epidemic modeling. Data-driven models of infectious diseases are increasingly used to forecast the evolution of an ongoing outbreak [1, 7, 27]. But very few models can mimic the internal mechanism of a stochastic simulator and answer “what-if questions” for pandemics with very different characteristics. Recently, [33] propose to use Gaussian process (GPs) as a prior for a SEIR compartmental model for learning lockdown policy effects, but GPs are computationally expensive and the simple SEIR model cannot capture the real-world large-scale, spatiotemporal epidemic dynamics considered in this work.

4 Experiments

We first compare the performance of INP with Gaussian Process using a simple susceptible-exposed-infectious-removed (SEIR) compartmental model for validation. Then we compare different acquisition functions for Bayesian active learning. Finally, we apply our INP model to mimic the dynamics of Local Epidemic and Mobility model (LEAM-US) simulator and compare the performance among different acquisition functions for Bayesian active learning.

4.1 SEIR Compartmental Model

SEIR Simulation. To show that INP indeed provides a more flexible and faster alternative to GP, we begin with a simple stochastic, discrete, chain-binomial SEIR compartmental model as our stochastic simulator, details of the model are deferred to the Appendix.

We set the total population N , where $N = S + E + I + R$, equal to 100,000, the initial number of exposed individuals equal to $E_0 = 2,000$, the initial number of infectious individuals equal to $E_0 = 2,000$, the latent period equal to 3 days ($\mu = 1/3$), the infectious period equal to 1 day ($\varepsilon = 1/1$), and we let the basic reproduction number R_0 (which in this case coincides with the transmissibility rate β) vary between 1.1 and 4.0 (step 0.05). Here, each R_0 corresponds to a specific scenario, which determines the parameters θ . Lastly, we simulate the first 50 days of the epidemic and generate 50 samples for each scenario.

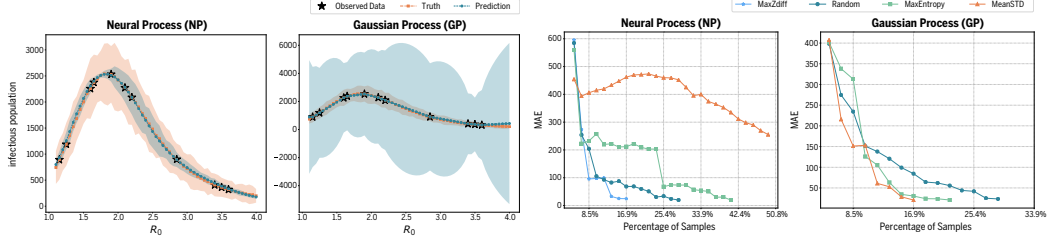


Figure 3: Neural Process vs. Gaussian Process for Bayesian active learning. Left: uncertainty quantification comparison with the truth. Right: MAE loss versus the percentage of samples for both NP and GP on the SEIR simulator

Model Implementation. We use both GP and INP to mimic the SEIR simulator. In this simplified experiment, we only predict the number of individuals in the infectious compartment at time t . The input is R_0 and the output is the 50 days’ infection prediction. We implement GP using `gpytorch MultitaskGPModel` [11] with Matern kernel. We trained GP model for 300 steps with learning rate fixed at 10^{-1} . As the simulator is simple, we implement a vanilla NP model with two fully-connected layers for the encoder and the decoder. The dimension of latent vector z is set at 4. We use Adam optimizer and use early stopping with patience fixed at 1000 epoch. The learning rate is fixed at 10^{-3} . For each epoch, it randomly selects 25% samples as context. The model is implemented by `pytorch` [31].

Uncertainty Quantification. Figure 3 compares the NP and GP performance on day 21 prediction. It shows the predicted number of infectious population for different R_0 and their confidence intervals (CI) with 10 standard deviations. We observe that both models fit the simulation dynamics well for mean predictions. However, NP has closer CIs to the truth, reflecting the simulator’s intrinsic uncertainty. GP shows larger CIs which represent the model’s own uncertainty.

Acquisition Functions. We compare different acquisition functions in Bayesian active learning. For the initial iteration, we train with the samples from three fixed scenarios selected randomly. Then we continue adding samples from the remaining scenarios to the training set until the validation loss converges. GP is not a latent variable model, hence MaxZdiff does not apply. We compute the L2 distance of the mean and standard deviation for MaxZdiff. We conduct random sampling three times with different random seeds to measure the average performance. We report the test loss using mean absolute error (MAE). The test set includes 59 different scenarios in the search space.

Figure 3 shows that random sampling converges similarly for NP and GP. Mean STD and Maximum Entropy are more sample efficient in GP, with Mean STD being 41.3% more sample efficient than random sampling. However, on neural processes, both methods are worse than random sampling while our proposed method MaxZdiff excels. This also validates our theory that the uncertainty of the deep surrogate model is better measured on the latent space instead of the predictions. . MaxZdiff takes only 16.9% of samples to converge, which is as efficient as Mean STD on GP. Mean STD fails to converge after using 49.2% of the samples.

Exploration Exploitation Trade-off. To understand why there is a large performance gap for MaxEntropy and Mean STD on GP vs. NP, we visualize the predictions for each Bayesian active learning iteration, shown in Figure 4 and Figure 5. For GP, both Mean STD and MaxEntropy depend on the model’s predictive uncertainty. Hence, with a small number of iterations ($I = 7$), they have already selected the scenarios including important information of the search space. However, For NP, its uncertainty reflects the intrinsic uncertainty of the simulator, rather than the NP model itself. Using predictive uncertainty tends to be over-conservative and without much exploration. MaxZdiff solves this problem by exploiting the uncertainty in the latent process and encouraging exploration. Its active learning behavior is similar to what Mean STD selected on GP.

4.2 Local Epidemic and Mobility model (LEAM-US)

As a real-world experiment, we use a large-scale, spatiotemporal, age-structured epidemic model, LEAM-US, as our stochastic simulator. Our goal is to design INP to mimic the internal mechanism of this simulator to accelerate disease modeling.

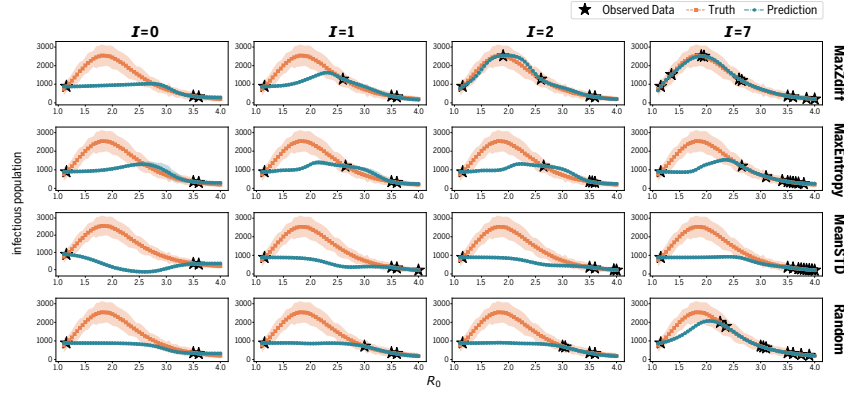


Figure 4: Acquisition functions on NP over 7 iterations. Predicted infectious population over R_0 .

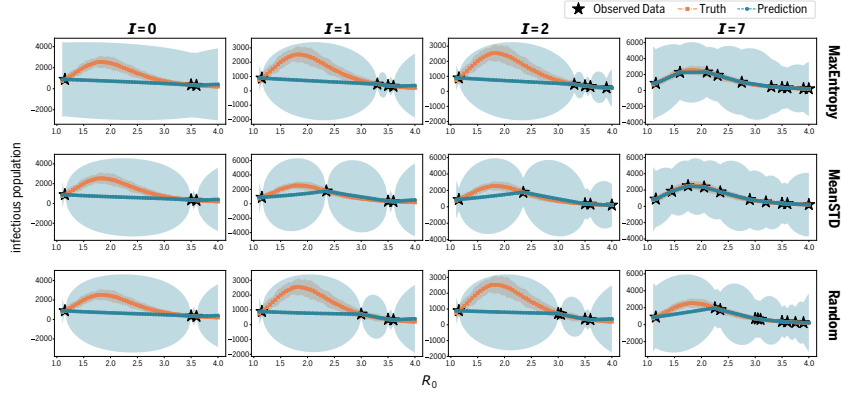


Figure 5: Comparison among acquisition functions on GP over 7 iterations. Predicted infectious population over different R_0 .

LEAM-US Simulator. The Local Epidemic and Mobility model (LEAM-US) is a stochastic, spatial, age-structured epidemic model based on a metapopulation approach which divides the United States in more than 3,100 subpopulations, each one corresponding to a different US county or statistically equivalent entity. Population size and county-specific age distributions reflect Census’ annual resident population estimates for year 2019. We consider individuals divided into 10 age groups: [0-9, 10-19, 20-24, 25-29, 30-39, 40-49, 50-59, 60-69, 70-79, 80+]. Contact mixing patterns are age-dependent and state specific and modeled considering contact matrices that describe the interaction of individuals in different social settings, namely: households, schools, workplaces, and contacts occurring in the general community [29]. LEAM-US integrates a human mobility layer, represented as a network, using both short-range (i.e., commuting) and long-range (i.e., flights) mobility data. The disease dynamics are modeled using a classic SEIR-like model and initial conditions are determined using the Global and Epidemic Mobility model [3, 4, 40, 42] calibrated to realistically represent the evolution of the COVID-19 pandemic [6, 8]. Lastly, travel restrictions, mobility reductions, and government interventions are explicitly modeled to mimic the real timeline of interventions of the events that occurred during the COVID-19 pandemic.

Dataset. We separate data monthly to predict the 28 days’ sequence from the 2nd to the 29th day of each month. We use data from March to November as training set and divide the December data into two halves for testing and validation. We first perform offline learning to show that the STNP model can learn the dynamics of LEAM-US. For Bayesian active learning, we use the training dataset as the search space. There are 45 different scenarios for each month. Overall, there are 360 scenarios in the search space, corresponding to 360 different θ with 18576 samples.

Model Implementation. We use INP with STNP to mimic the internal mechanism of LEAM-US. As is shown in Figure 2, the input $\theta_{1:t}$ is the county-level parameters for LEAM-US with a dimension of 10. The county level embedding uses 1 layer DCGRU with a width of 16. The internal state is at state level with dimension of 16. The state level encoder and decoder use 3 layer GRUs with width of 128. The dimension of the latent process $z_{1:t}$ is 32. The dimension of output $x_{1:t}$ is 24, including the incidence and prevalence for 12 compartments. We trained STNP model for 300 steps with learning

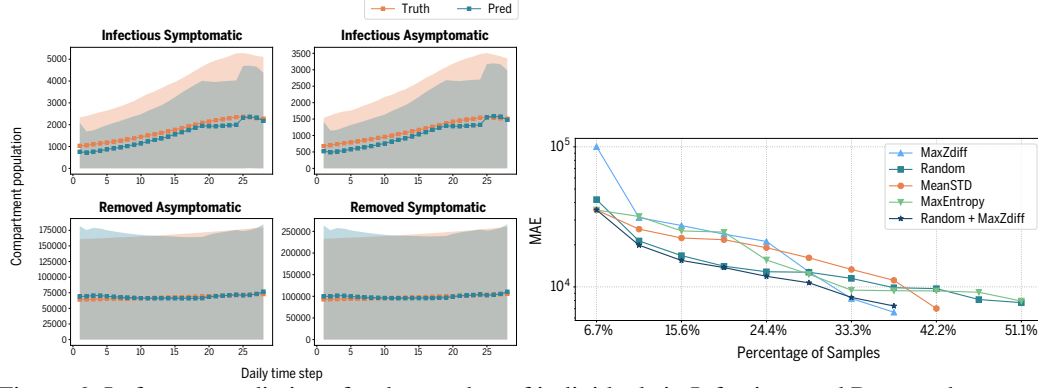


Figure 6: Left: INP predictions for the number of individuals in Infectious and Removed compartments in LEAM-US model. Right: acquisition function comparisons on the LEAM-US simulator. MAE loss versus the percentage of samples for INP during Bayesian active learning.

rate fixed at 10^{-3} using Adam optimizer. We perform early stopping with 50 patience for offline learning, and with 80 patience for Bayesian active learning. For each epoch, it randomly selects 25% samples as context. The model is implemented by pytorch.

STNP Predictions. The left side of Figure 6 visualize the STNP predictions in four key compartments of a typical scenario with $R_0 = 2.25$ from December 2nd to December 29th. The confidence interval is plotted with 2 standard deviations. We can see that both the mean and confidence interval of STNP predictions match the truth well. These results demonstrate the promise that the generative STNP model can serve as a deep surrogate model for the LEAM-US simulator.

Acquisition Functions. We compare different acquisition functions in Bayesian active learning. For the initial iteration, we train with 8 scenarios from March to November with the same randomly selected R_0 . Then we continue adding 16 scenarios to the training set until the validation loss converges. We use Mean STD, Maximum Entropy, MaxZdiff, the combined method with random sampling for the first two iterations plus MaxZdiff for the rest of the iterations, and compare them with random sampling as baseline. We conduct random sampling three times with different random seeds to measure the average performance. MAE is used for test loss. The test set includes 360 scenarios in the search space.

The right side of Figure 6 shows the log scale MAE versus the percentage of samples included for training, which is linear associated with the computation power. Both MaxZdiff and the combined method take 37.7% of the samples to converge, while Mean STD takes 42.2% to converge. Both random sampling and Maximum Entropy take 51.1% to converge. We notice that random sampling with more exploration in the early iterations has a slight advantage. Therefore, we also combine the two acquisition functions, leading to the hybrid method Random-MaxZdiff. From the figure, we can see that this hybrid method is optimal during the entire learning process until convergence.

5 Conclusion & Limitation

We present a new way to seamlessly interact with existing stochastic simulators and accelerate simulation. Our Neural Interactive Process (INP) includes a novel spatiotemporal neural process model to approximate the underlying simulation dynamics. It infers the latent process which describes the intrinsic uncertainty of the simulator. We exploit this uncertainty and propose max-z-difference as an acquisition function in Bayesian active learning. We perform theoretical analysis and demonstrate that our approach reduces sample complexity compared with random sampling in high dimension. Using a complex epidemic simulator, we demonstrate our method provides a faster and more flexible alternative to Gaussian process for policy optimization and scenario creation.

One limitation of our current work is the optimization step. Currently, we use a brute force search mechanism to select the parameters according to the value of an acquisition function. However, this search will become expensive in the high dimension. We plan to leverage Monte Carlo sampling and

Bayesian optimization techniques to parameterize the reward function. Then we would also be able to directly optimize for the target parameters with auto-differentiation.

Broader Impact

Stochastic simulation plays a fundamental role in science. Accelerating scientific simulation is the most important step towards the long-term goal of AI for science. We believe our method possesses broader interests in computational modeling far beyond infectious disease simulation. For similar simulations such as simulating multi-agent behavior in social science, as well as molecular dynamics simulations in chemistry and materials science, we can easily replicate our interactive process and transfer the setting to impact broader applications in many related scientific fields.

One ethical challenge of our framework is data privacy. The mobility data used in this study are aggregated and privacy-enhanced mobility data for academic research and humanitarian initiatives. These first-party data are collected from users who have opted in to provide access to their GPS location data anonymously, through a GDPR-compliant framework. Furthermore, in our analysis the geospatial information is used only to create a series of co-location events that are used as proxy for human-to-human contacts.

Acknowledgement

This work was supported in part by JP Morgan Outstanding Faculty Award, AWS Machine Learning Research Award, Google Faculty Award, NSF Grant #2037745, and the DARPA W31P4Q-21-C-0014. D.W. acknowledges support from the HDSI Ph.D. Fellowship. M.C. and A.V. acknowledge support from grants HHS/CDC 5U01IP0001137 and HHS/CDC 6U01IP001137. The findings and conclusions in this study are those of the authors and do not necessarily represent the official position of the funding agencies, the National Institutes of Health, or the U.S. Department of Health and Human Services.

References

- [1] S. Arik, C.-L. Li, J. Yoon, R. Sinha, A. Epshteyn, L. Le, V. Menon, S. Singh, L. Zhang, M. Nikoltchev, et al. Interpretable sequence learning for covid-19 forecasting. *Advances in Neural Information Processing Systems*, 33, 2020.
- [2] S. Asmussen and P. W. Glynn. *Stochastic simulation: algorithms and analysis*, volume 57. Springer Science & Business Media, 2007.
- [3] D. Balcan, V. Colizza, B. Gonçalves, H. Hu, J. J. Ramasco, and A. Vespignani. Multiscale mobility networks and the spatial spreading of infectious diseases. *Proceedings of the National Academy of Sciences*, 106(51):21484–21489, 2009.
- [4] D. Balcan, B. Gonçalves, H. Hu, J. J. Ramasco, V. Colizza, and A. Vespignani. Modeling the spatial spread of infectious diseases: The global epidemic and mobility computational model. *Journal of computational science*, 1(3):132–145, 2010.
- [5] Z. Chen and J. J. Dongarra. Condition numbers of gaussian random matrices. *SIAM Journal on Matrix Analysis and Applications*, 27(3):603–620, 2005.
- [6] M. Chinazzi, J. T. Davis, M. Ajelli, C. Gioannini, M. Litvinova, S. Merler, A. P. y Piontti, K. Mu, L. Rossi, K. Sun, et al. The effect of travel restrictions on the spread of the 2019 novel coronavirus (covid-19) outbreak. *Science*, 2020.
- [7] E. Y. Cramer, V. K. Lopez, J. Niemi, G. E. George, J. C. Cegan, I. D. Dettwiller, W. P. England, M. W. Farthing, R. H. Hunter, B. Lafferty, et al. Evaluation of individual and ensemble probabilistic forecasts of covid-19 mortality in the us. *medRxiv*, 2021.
- [8] J. T. Davis, M. Chinazzi, N. Perra, K. Mu, A. Pastore y Piontti, M. Ajelli, N. E. Dean, C. Gioannini, M. Litvinova, S. Merler, L. Rossi, K. Sun, X. Xiong, M. E. Halloran, I. M. Longini, C. Viboud, and A. Vespignani. Estimating the establishment of local transmission and the cryptic phase of the covid-19 pandemic in the usa. *medRxiv*, 2020.
- [9] S. Du, J. Lee, H. Li, L. Wang, and X. Zhai. Gradient descent finds global minima of deep neural networks. In *Proceedings of the 36th International Conference on Machine Learning (ICML)*, pages 1675–1685, 2019.
- [10] Y. Gal, R. Islam, and Z. Ghahramani. Deep bayesian active learning with image data. In *International Conference on Machine Learning*, pages 1183–1192. PMLR, 2017.

- [11] J. R. Gardner, G. Pleiss, D. Bindel, K. Q. Weinberger, and A. G. Wilson. Gpytorch: Blackbox matrix-matrix gaussian process inference with gpu acceleration. *arXiv preprint arXiv:1809.11165*, 2018.
- [12] M. Garnelo, J. Schwarz, D. Rosenbaum, F. Viola, D. J. Rezende, S. Eslami, and Y. W. Teh. Neural processes. *arXiv preprint arXiv:1807.01622*, 2018.
- [13] D. T. Gillespie. Stochastic simulation of chemical kinetics. *Annu. Rev. Phys. Chem.*, 58:35–55, 2007.
- [14] F. Götze and A. Tikhomirov. Rate of convergence in probability to the Marchenko-Pastur law. *Bernoulli*, 10(3):503 – 548, 2004.
- [15] T. Hale, N. Angrist, R. Goldszmidt, B. Kira, A. Petherick, T. Phillips, S. Webster, E. Cameron-Blake, L. Hallas, S. Majumdar, and H. Tatlow. A global panel database of pandemic policies (Oxford COVID-19 Government Response Tracker). *Nature Human Behaviour*, 2021.
- [16] P. Holl, N. Thuerey, and V. Koltun. Learning to control pdes with differentiable physics. In *International Conference on Learning Representations*, 2019.
- [17] N. Houlsby, F. Huszár, Z. Ghahramani, and M. Lengyel. Bayesian active learning for classification and preference learning. *arXiv preprint arXiv:1112.5745*, 2011.
- [18] IATA, International Air Transport Association, 2021. <https://www.iata.org/>.
- [19] H. Kim, A. Mnih, J. Schwarz, M. Garnelo, A. Eslami, D. Rosenbaum, O. Vinyals, and Y. W. Teh. Attentive neural processes. *International Conference on Learning Representation*, 2019.
- [20] D. P. Kingma and M. Welling. Auto-encoding variational bayes. *arXiv preprint arXiv:1312.6114*, 2013.
- [21] B. Lakshminarayanan, A. Pritzel, and C. Blundell. Simple and scalable predictive uncertainty estimation using deep ensembles. *NeurIPS*, 2017.
- [22] D. Lamberton and B. Lapeyre. *Introduction to stochastic calculus applied to finance*. CRC press, 2007.
- [23] Y. Li, R. Yu, C. Shahabi, and Y. Liu. Diffusion convolutional recurrent neural network: Data-driven traffic forecasting. *arXiv preprint arXiv:1707.01926*, 2017.
- [24] Y. Li, R. Yu, C. Shahabi, and Y. Liu. Diffusion convolutional recurrent neural network: Data-driven traffic forecasting. In *International Conference on Learning Representations (ICLR)*, 2018.
- [25] G. LLC. "Google COVID-19 Community Mobility Reports". <https://www.google.com/covid19/mobility/>.
- [26] C. Louizos, X. Shi, K. Schutte, and M. Welling. The functional neural process. *Advances in Neural Information Processing Systems*, 2019.
- [27] J. Lourenco, R. Paton, M. Ghafari, M. Kraemer, C. Thompson, P. Simmonds, P. Klenerman, and S. Gupta. Fundamental principles of epidemic spread highlight the immediate need for large-scale serological surveys to assess the stage of the sars-cov-2 epidemic. *MedRxiv*, 2020.
- [28] S. Mei and A. Montanari. The generalization error of random features regression: Precise asymptotics and double descent curve. *arXiv: 1908.05355*, 2019.
- [29] D. Mistry, M. Litvinova, M. Chinazzi, L. Fumanelli, M. F. Gomes, S. A. Haque, Q.-H. Liu, K. Mu, X. Xiong, M. E. Halloran, et al. Inferring high-resolution human mixing patterns for disease modeling. *arXiv preprint arXiv:2003.01214*, 2020.
- [30] OAG, Aviation Worldwide Limited, 2021. <http://www.oag.com/>.
- [31] A. Paszke, S. Gross, F. Massa, A. Lerer, J. Bradbury, G. Chanan, T. Killeen, Z. Lin, N. Gimelshein, L. Antiga, et al. Pytorch: An imperative style, high-performance deep learning library. In *Advances in neural information processing systems*, pages 8026–8037, 2019.
- [32] R. Pestourie, Y. Mroueh, T. V. Nguyen, P. Das, and S. G. Johnson. Active learning of deep surrogates for pdes: Application to metasurface design. *npj Computational Materials*, 6(1):1–7, 2020.
- [33] Z. Qian, A. M. Alaa, and M. van der Schaar. When and how to lift the lockdown? global covid-19 scenario analysis and policy assessment using compartmental gaussian processes. *Advances in Neural Information Processing Systems*, 33, 2020.
- [34] S. Rasp, M. S. Pritchard, and P. Gentine. Deep learning to represent subgrid processes in climate models. *Proceedings of the National Academy of Sciences*, 115(39):9684–9689, 2018.
- [35] B. D. Ripley. *Stochastic simulation*, volume 316. John Wiley & Sons, 2009.
- [36] A. Sanchez-Gonzalez, J. Godwin, T. Pfaff, R. Ying, J. Leskovec, and P. Battaglia. Learning to simulate complex physics with graph networks. In *International Conference on Machine Learning*, pages 8459–8468. PMLR, 2020.
- [37] Y. Shen, H. Yun, Z. C. Lipton, Y. Kronrod, and A. Anandkumar. Deep active learning for named entity recognition. In *Proceedings of the 2nd Workshop on Representation Learning for NLP*, pages 252–256, 2017.

- [38] A. Siddhant and Z. C. Lipton. Deep bayesian active learning for natural language processing: Results of a large-scale empirical study. *arXiv preprint arXiv:1808.05697*, 2018.
- [39] J. Snoek, O. Rippel, K. Swersky, R. Kiros, N. Satish, N. Sundaram, M. Patwary, M. Prabhat, and R. Adams. Scalable bayesian optimization using deep neural networks. In *International conference on machine learning*, pages 2171–2180. PMLR, 2015.
- [40] M. Tizzoni, P. Bajardi, C. Poletto, J. J. Ramasco, D. Balcan, B. Gonçalves, N. Perra, V. Colizza, and A. Vespignani. Real-time numerical forecast of global epidemic spreading: case study of 2009 a/h1n1pdm. *BMC medicine*, 10(1):165, 2012.
- [41] R. Wang, K. Kashinath, M. Mustafa, A. Albert, and R. Yu. Towards physics-informed deep learning for turbulent flow prediction. In *Proceedings of the 26th ACM SIGKDD international conference on Knowledge discovery and data mining. ACM, 2020*, 2020.
- [42] Q. Zhang, K. Sun, M. Chinazzi, A. P. y Piontti, N. E. Dean, D. P. Rojas, S. Merler, D. Mistry, P. Poletti, L. Rossi, et al. Spread of Zika virus in the Americas. *Proceedings of the National Academy of Sciences*, 114(22):E4334–E4343, 2017.
- [43] C. Zimmer, M. Meister, and D. Nguyen-Tuong. Safe active learning for time-series modeling with gaussian processes. In *Proceedings of the 32nd International Conference on Neural Information Processing Systems*, pages 2735–2744, 2018.

A Theoretical Analysis

From the main text we know that in each round, the output random variable

$$X = \langle \Psi(\theta), z^* \rangle + \epsilon. \quad (3)$$

We further assume that the random noise ϵ is mean zero and σ -subGaussian.

Using this information, we treat z as an unknown parameter and define a likelihood function so that $p(X|z; \theta)$ has good coverage over the observations:

$$p(X_k|z; \theta_k) \propto \exp \left(-\frac{1}{2\sigma^2} (X_k - \langle \Psi(\theta_k), z \rangle)^2 \right).$$

Let the prior distribution over z be $p(z|\theta_k) = p(z) \propto \exp \left(-\frac{m}{2\sigma^2} \|z\|^2 \right)$. Here we use k instead of (i) in the Algorithm 1 to represent the number of iterations. We can form a posterior over z in the k -th round:

$$p(z|X_1, \theta_1, \dots, X_k, \theta_k) \propto \exp \left(-\frac{m}{2\sigma^2} \|z\|^2 - \frac{1}{2\sigma^2} \sum_{s=1}^k (X_s - \langle \Psi(\theta_s), z \rangle)^2 \right).$$

Focusing on the random variable $z \sim p(\cdot|X_1, \theta_1, \dots, X_k, \theta_k)$, the estimate of the hidden variable, we can express it at k -th round as:

$$z_k = \hat{z}_k + \sigma V_k^{-1} \eta_k, \quad (4)$$

where $\hat{z}_k = V_k^{-1} \sum_{s=1}^k X_s \Psi(\theta_s)$, $V_k = mI + \sum_{s=1}^k \Psi(\theta_s) \Psi(\theta_s)^T$, and η_k is a standard normal random variable.

We can either choose action θ randomly or greedily. A random choice of θ corresponds to taking

$$\theta_k \sim \mathcal{N}(0, I), \quad (5)$$

A greedy procedure is to choose action θ_k in the k -th round so that the variance of the prediction is the greatest:

$$\theta_k = \arg \max_{\theta \in \mathbb{R}^d} \mathbb{E}_{z \sim p(\cdot|X_1, \theta_1, \dots, X_{k-1}, \theta_{k-1})} \left[\left(\langle \Psi(\theta), z \rangle - \mathbb{E}_{z \sim p(\cdot|X_1, \theta_1, \dots, X_{k-1}, \theta_{k-1})} \langle \Psi(\theta), z \rangle \right)^2 \right]. \quad (6)$$

For both approaches, we assume that the features $\Psi(\theta)$ are normalized.

We compare the statistical risk of this approach with the random sampling approach.

Assume that the features are normalized, so that for all $\theta \in \mathbb{R}^d$, $\Psi(\theta) \in \mathbb{S}^{d-1}$. Define a matrix $A_k \in \mathbb{R}^{d \times k}$ containing all the column vectors $\{\Psi(\theta_1), \dots, \Psi(\theta_k)\}$. We can then express the estimation error in the following lemma.

Lemma 1. *The estimation error $\|\hat{z}_k - z^*\|_2$ can be bounded as follow.*

$$\begin{aligned} \|\hat{z}_k - z^*\|_2 &\leq m \left(m + \sigma_{\min} (A_k A_k^T) \right)^{-1} \cdot \|z^*\|_2 \\ &\quad + \min \left\{ 1/(2\sqrt{m}), 1/\left(\sqrt{\sigma_{\min} (A_k A_k^T)} + \frac{m}{\sqrt{\sigma_{\min} (A_k A_k^T)}} \right) \right\} \cdot \sigma\sqrt{d}. \end{aligned}$$

We now analyze random sampling of θ versus greedy search for θ .

If the feature map $\Psi(\cdot) = \text{id}$, then from random matrix theory, we know that for θ randomly sampled from a normal distribution and normalized to $\|\theta\| = 1$, $\sigma_{\min} (\frac{1}{k} A_k A_k^T)$ will converge to $(\sqrt{1/k} - \sqrt{1/d})^2$ for large k , which is of order $\Omega(1/d)$. This will lead to an appealing risk bound for $\|\hat{z}_k - z^*\|_2$ on the order of $\mathcal{O}(d/\sqrt{k})$.

However, in high dimension, this feature map is often far from identity. In the proof of Theorem 1 below, we demonstrate that even when $\Psi(\cdot)$ is simply a linear random feature map, with i.i.d. normal entries, random exploration in θ can lead to deteriorated error bound. This setting is motivated by the analyses in wide neural networks, where the features learned from gradient descent are close to those generated from random initialization [9, 28].

Theorem 1 (Formal statement). *Assume that the noise ϵ in (3) is σ -subGaussian.*

For a normalized linear random feature map $\Psi(\cdot)$, greedily maximizing the variance of the posterior predictive distribution following (6) in search of θ will lead to an error $\|\hat{z}_k - z^\|_2 = \mathcal{O}(\sigma d/\sqrt{k})$ with high probability.*

On the other hand, random sampling of θ following (5) will lead to $\|\hat{z}_k - z^\|_2 = \mathcal{O}(\sigma d^2/\sqrt{k})$ with high probability.*

Proof of Theorem 1. For a linear random feature map, we can express $\Psi(\theta) = \Psi\theta$, where entries in $\Psi \in \mathbb{R}^{d \times d}$ are i.i.d. normal. The entries of $\Psi\theta$ are then normalized.

- For random exploration of θ , the matrix containing the feature vectors becomes $A_k = \Psi\Theta_k$, where matrix $\Theta_k \in \mathbb{R}^{d \times k}$ collects all the k column vectors of $\{\theta_1, \dots, \theta_k\}$. Then $A_k A_k^T = \Psi\Theta_k\Theta_k^T\Psi^T$. From random matrix theory, we know that the condition number of Ψ is equal to d with high probability [5]. Hence for normalized Ψ and θ , $\sigma_{\min}(\Psi\Theta_k\Theta_k^T\Psi^T) \geq \sigma_{\min}^2(\Psi)\sigma_{\min}(\Theta_k\Theta_k^T) = \frac{1}{d^2}\sigma_{\min}(\Theta_k\Theta_k^T)$. The inequality holds because the smallest singular value is the inverse of the norm of the inverse matrix.

We then use the fact from random matrix theory that for normalized random θ , the asymptotic distribution of the eigenvalues of $\frac{1}{k}\Theta_k\Theta_k^T$ follow the (scaled) Marchenko–Pastur distribution, which is supported on $\lambda \in \left[\left(\sqrt{1/k} - \sqrt{1/d}\right)^2, \left(\sqrt{1/k} + \sqrt{1/d}\right)^2\right]$, where the $1/d$ scaling comes from the fact that θ is normalized [14]. Hence for large k , $\sigma_{\min}(\Theta_k\Theta_k^T) \geq \left(1 - \sqrt{k/d}\right)^2$ with high probability. This combined with the previous paragraph yields that for the random feature model,

$$\sigma_{\min}(A_k A_k^T) = \Omega\left(\frac{1}{d^2} \left(1 - \sqrt{k/d}\right)^2\right)$$

with high probability. Plugging this result into Lemma 1, we obtain that the error $\|\hat{z}_k - z^*\|_2$ for random exploration in the space of θ is of order $\mathcal{O}(d^2/\sqrt{k})$.

- We then analyze the error associated with greedy maximization of the posterior predictive variance. We first note that the variance of the posterior predictive distribution in equation (6) can be expressed as follows using equation (4):

$$\mathbb{E}[(\langle \Psi(\theta), z \rangle - \mathbb{E}\langle \Psi(\theta), z \rangle)^2] = \sigma^2 \mathbb{E}[(\langle \Psi(\theta), V_{k-1}^{-1} \eta_k \rangle)^2] = \sigma^2 \Psi(\theta)^T V_{k-1}^{-2} \Psi(\theta), \quad (7)$$

where the expectations are with respect to $z \sim p(\cdot | X_1, \theta_1, \dots, X_{k-1}, \theta_{k-1})$.

We perform a singular value decomposition $A_k = U_k \Lambda_k W_k$. Then $\sum_{s=1}^k \Psi(\theta_s) \Psi(\theta_s)^T = A_k A_k^T = U_k \Lambda_k \Lambda_k^T U_k^T$, and that $V_{k-1}^{-2} = (mI + A_{k-1} A_{k-1}^T)^{-2} = U_{k-1} (mI + \Lambda_{k-1} \Lambda_{k-1}^T)^{-2} U_{k-1}^T$. Via this formulation, we see that maximizing $\Psi(\theta)^T V_{k-1}^{-2} \Psi(\theta)$ in equation (7) to choose θ_k is equivalent to choosing $\Psi(\theta_k) = (U_{k-1})_{(\cdot, l)}^T$, where $l = \arg \min_{i \in \{1, \dots, d\}} (\Lambda_{k-1} \Lambda_{k-1}^T)_{(i, i)}$. In words, when we use greedy method and maximize the variance of the prediction, it corresponds to taking $\Psi(\theta_k)$ in the direction of the smallest eigenvector of V_{k-1} .

Since every $\Psi(\theta)$ is normalized and we initialize uniformly: $V_0 = mI$, the process is equivalent to scanning the orthogonal spaces of normalized vectors in \mathbb{R}^d for $\lfloor k/d \rfloor$ times. For large k , entries in $\Lambda_k \Lambda_k^T$ are approximately uniform and are all larger than or equal to $\lfloor k/d \rfloor$. Then $\sigma_{\min}(A_k A_k^T) = \Omega(k/d)$. Plugging into the bound of Lemma 1, we obtain that

$$\|\hat{z}_k - z^*\|_2 = \mathcal{O}\left(\frac{\sigma d}{\sqrt{k}}\right).$$

□

Proof of Lemma 1. We first express the estimate \hat{z}_k as follows.

$$\hat{z}_k = V_k^{-1} \sum_{s=1}^k X_s \Psi(\theta_s) = V_k^{-1} \sum_{s=1}^k \Psi(\theta_s) \Psi(\theta_s)^T z^* + V_k^{-1} \sum_{s=1}^k \epsilon_s \Psi(\theta_s).$$

Then

$$\begin{aligned} \|\hat{z}_k - z^*\|_2 &= \left\| \left(V_k^{-1} \sum_{s=1}^k \Psi(\theta_s) \Psi(\theta_s)^T - I \right) z^* + V_k^{-1} \sum_{s=1}^k \epsilon_s \Psi(\theta_s) \right\|_2 \\ &\leq \underbrace{\left\| \left(V_k^{-1} \sum_{s=1}^k \Psi(\theta_s) \Psi(\theta_s)^T - I \right) z^* \right\|_2}_{T_1} + \underbrace{\left\| V_k^{-1} \sum_{s=1}^k \epsilon_s \Psi(\theta_s) \right\|_2}_{T_2}. \end{aligned}$$

Define a matrix $A_k \in \mathbb{R}^{d \times k}$ containing all the column vectors $\{\Psi(\theta_1), \dots, \Psi(\theta_k)\}$ and perform a singular value decomposition $A_k = U_k \Lambda_k W_k^T$. Then $\sum_{s=1}^k \Psi(\theta_s) \Psi(\theta_s)^T = A_k A_k^T = U_k \Lambda_k \Lambda_k^T U_k^T$, and $V_k = mI + A_k A_k^T$. We further define vector $e_k \in \mathbb{R}^s$ where $(e_k)_s = \epsilon_s$. We use this definition to simplify the two terms further.

For term T_1 ,

$$\begin{aligned} \left\| \left(V_k^{-1} \sum_{s=1}^k \Psi(\theta_s) \Psi(\theta_s)^T - I \right) z^* \right\|_2 &= m \|V_k^{-1} z^*\|_2 \\ &\leq m \|V_k^{-1}\|_2 \cdot \|z^*\|_2 \\ &= m \left(m + \sigma_{\min}(A_k A_k^T) \right)^{-1} \cdot \|z^*\|_2. \end{aligned}$$

For term T_2 , we define a diagonal matrix $\bar{\Lambda}_k \in \mathbb{R}^{k \times k}$ which satisfies $(\bar{\Lambda}_k)_{i,i} = 1$ if $i \leq d$ and $(\bar{\Lambda}_k)_{i,i} = 0$ if $i > d$, when $k > d$. The following bound on T_2 can be achieved.

$$\begin{aligned} \left\| V_k^{-1} \sum_{s=1}^k \epsilon_s \Psi(\theta_s) \right\|_2 &= \|V_k^{-1} A_k e_k\|_2 \\ &= \left\| U_k \left(\Lambda_k \Lambda_k^T + mI \right)^{-1} U_k^T U_k \Lambda_k \bar{\Lambda}_k W_k e_k \right\|_2 \\ &\leq \left\| U_k \left(\Lambda_k \Lambda_k^T + mI \right)^{-1} \Lambda_k \right\|_2 \cdot \|\bar{\Lambda}_k W_k e_k\|_2 \\ &= \left\| \left(\Lambda_k \Lambda_k^T + mI \right)^{-1} \Lambda_k \right\|_2 \cdot \|\bar{\Lambda}_k W_k e_k\|_2 \\ &\leq \min \left\{ 1/(2\sqrt{m}), 1/\left(\sqrt{\sigma_{\min}(A_k A_k^T)} + \frac{m}{\sqrt{\sigma_{\min}(A_k A_k^T)}} \right) \right\} \cdot \|\bar{\Lambda}_k W_k e_k\|_2. \end{aligned}$$

Assuming that noise ϵ_s is σ -subGaussian, then so is $W_k e_k$ since W_k is a unitary matrix. Multiplied by the diagonal matrix $\bar{\Lambda}_k$ which has zero, $\|\bar{\Lambda}_k W_k e_k\|_2 \leq \sigma \sqrt{d}$. Therefore,

$$\left\| V_k^{-1} \sum_{s=1}^k \epsilon_s \Psi(\theta_s) \right\|_2 \leq \min \left\{ 1/(2\sqrt{m}), 1/\left(\sqrt{\sigma_{\min}(A_k A_k^T)} + \frac{m}{\sqrt{\sigma_{\min}(A_k A_k^T)}} \right) \right\} \cdot \sigma \sqrt{d}.$$

□

B Experiment Details

B.1 SEIR Model Details

We begin with a simple stochastic, discrete, chain-binomial SEIR compartmental model as our stochastic simulator. In this model, susceptible individuals (S) become exposed (E) through interactions with infectious individuals (I). Exposed individuals which are infected but not yet infectious transition to infectious compartment at a rate ε that is inversely proportional to the latent period of the disease. Lastly, infectious individuals transition to the removed compartment at a rate μ which is inversely proportional to the infectious period. Removed individuals (R) are assumed to be no longer infectious and they are to be considered either recovered or dead. All transitions are simulated using a chain-binomial approach in which the number of transitions is randomly drawn from a binomial distribution.

B.2 LEAM-US Model Details

LEAM-US integrates a human mobility layer, represented as a network, using both short-range (i.e., commuting) and long-range (i.e., flights) mobility data. Commuting flows between counties are obtained from the 2011-2015 5-Year ACS Commuting Flows survey and properly adjusted to account for differences in population totals since the creation of the dataset. Instead, long-range air traveling flows are quantified using origin-destination daily passenger flows between airport pairs as reported by the Official Aviation Guide (OAG) and IATA databases (updated in 2021) [30, 18]. In addition, flight probabilities are age and country specific.

The model is initialized using a multi-scale modeling approach that utilizes GLEAM, the Global and Epidemic Mobility model [3, 4, 40, 42, 6, 8], to simulate a set of 500 different initial conditions for LEAM-US starting on February 16th, 2020. The disease dynamics are modeled using a classic SEIR-like model as in the first experiment and the time interval considered for the simulations is February 2020 until December 2020. However, in this

Table 1: Performance comparison of different acquisition functions in INP model for SEIR simulator

Percentage of samples	MaxZdiff	Random	MeanSTD	MaxEntropy
6.8%	342.58 \pm 68.16	254.06 \pm 44.95	557.99 \pm 121.24	394.96 \pm 127.6
10.2%	115.63 \pm 20.33	105.41 \pm 22.51	364.22 \pm 35.94	188.11 \pm 49.62
13.6%	42.99 \pm 14.65	82.7 \pm 16.42	377.35 \pm 39.83	140.24 \pm 79.52
16.9%	38.35 \pm 19.76	68.45 \pm 27.02	392.73 \pm 49.27	135.39 \pm 80.44

Table 2: Performance comparison of different acquisition functions in GP model for SEIR simulator

Percentage of samples	Random	MeanSTD	MaxEntropy
6.8%	274.53 \pm 29.56	234.04 \pm 26.	453.67 \pm 91.07
10.2%	150.97 \pm 19.58	122.94 \pm 21.3	183.52 \pm 41.02
13.6%	120.59 \pm 37.01	47.81 \pm 4.38	85.84 \pm 19.98
16.9%	84.49 \pm 20.2	23.48 \pm 2.05	56.98 \pm 19.28

second model, travel restrictions, mobility reductions, and government interventions are explicitly modeled to mimic the real timeline of interventions of the events that occurred during the COVID-19 pandemic. Specifically, Google’s COVID-19 Community Mobility Reports [25] are used to quantify mobility and contact reductions, while non-pharmaceutical interventions and other policy interventions are tracked using the Oxford Covid-19 Government Response Tracker (OxCGRT) [15].

B.3 Implementation Details

For both GP and INP model mimicking SEIR simulation, we ran experiments using Google Colab. No GPU accelerator is needed for this simple model. It takes 60 min and 30 min to converge separately. For INP model mimicking LEAM-US simulation, we ran experiments with GEFORCE RTX 2080. It takes one day for the training to converge. For all experiments, we run with three different random seeds.

C Additional Results

C.1 Offline Model

For the left side of Figure 6, the corresponding Weighted Mean Absolute Percentage Error (WMAPE) are 0.136, 0.134, 0.03, and 0.027 for infectious symptomatic, infectious asymptomatic, removed asymptomatic, and removed symptomatic compartments respectively.

C.2 INP Model and GP Model

Table 1 shows the average results together with the standard deviation of INP model for SEIR simulator after running experiments three times. It shows random sampling has a slight advantage in the early iterations and MaxZdiff takes back the advantage after using 13.6% of samples. Similarly, in Table 3, INP model for LEAM-US simulator, Random-maxZdiff has similar performance as random sampling in the early iterations. However, either Random-maxZdiff or MaxZdiff becomes optimal with the percentage of samples from 24.4% to 42.2%. Table 2 shows the average results together with the standard deviation of GP model for SEIR simulator. It can be found that MeanSTD always has the best performance.

Table 3: Performance comparison of different acquisition functions in INP model for LEAM-US simulator, population divided by 1000.

Percentage of samples	Random	MeanSTD	MaxEntropy	MaxZdiff	Random + MaxZdiff
6.7%	32.616 \pm 6.948	36.08 \pm 3.642	35.660 \pm 0.879	102.593 \pm 4.002	32.071 \pm 2.354
15.6%	17.029 \pm 1.42	24.796 \pm 5.963	26.699 \pm 1.833	25.617 \pm 1.512	18.061 \pm 2.327
24.4%	13.474 \pm 0.487	18.616 \pm 3.466	14.452 \pm 0.684	20.187 \pm 1.815	13.408 \pm 1.273
33.3%	11.001 \pm 0.349	13.028 \pm 0.942	10.896 \pm 1.143	10.238 \pm 1.909	11.455 \pm 2.102
42.2%	8.725 \pm 0.615	7.792 \pm 0.88	8.024 \pm 1.396	7.058 \pm 1.13	8.786 \pm 1.689